Effects of Nanoscale Hydroxypropyl Lignin on Properties of Soy Protein Plastics

Pu Chen,[1,2] Lina Zhang,[1,2] Shuping Peng,[3] Bing Liao[3]

[1]*Department of Chemistry, Wuhan University, Wuhan 430072, People's Republic of China*
[2]*Center of Nanoscience and Nanotechnology, Wuhan University, Wuhan 430072, People's Republic of China*
[3]*Key Laboratory of Cellulose Chemistry, Guangzhou Institute of Chemistry, Chinese Academy of Sciences, Guangzhou 510650, People's Republic of China*

Received 30 December 2004; accepted 31 October 2005
DOI 10.1002/app.23755
Published online in Wiley InterScience (www.interscience.wiley.com).

ABSTRACT: For the first time, soy protein isolate (SPI)/hydroxypropyl alkaline lignin (HPL) composites have been successfully prepared by mixing them in aqueous solution containing a small amount of glutaraldehyde as compatibilizer, and then compression-molded to obtain plastic sheets. The structures of the SPI/HPL composites were characterized by Fourier transform infrared spectroscopy, X-ray diffraction, transmission electron microscopy, and scanning electron microscopy, indicating the existence of amorphous networks and nanoscale HPL dispersion in the SPI matrix. When HPL content was lower than 6 wt %, the HPL-domain occurred in SPI/HPL composites with a dimension of about 50 nm, indicating a high interfacial activity. Differential scanning calorimetry analysis showed that the glass transition temperature of the SPI/HPL sheets increased from 62.5 to 70.4°C with an increase of HPL content from 0 to 6 wt %. Moreover, the tensile strength of the SPI/HPL nanocomposite sheets with 6 wt % HPL and 3.3 wt % glutaraldehyde was enhanced from 8.4 to 23.1 MPa compared with that of the SPI sheets, suggesting that the nanoscale HPL dispersion significantly reinforced the SPI materials. © 2006 Wiley Periodicals, Inc. J Appl Polym Sci 101: 334–341, 2006

Key words: biodegradable plastics; soy protein isolate; hydroxypropyl alkaline lignin; glutaraldehyde; compatibilization; reinforce

INTRODUCTION

In the last decades, the development of biodegradable polymer, based on renewable resources, has been of growing concern because of environmental pollution and the petroleum crisis.[1] Soy protein, as a readily available biopolymer and potential renewable source for biodegradable plastics, has attracted much attention.[2,3] It is noted that plastics made from soy protein alone possess good biodegradability but have poor flexibility,[4,5] and so a plasticizer is usually used to overcome the brittleness of soy protein plastics, which unavoidably leads to a significant decrease in tensile strength.[6] To obtain flexible soy protein isolate (SPI) plastics with high tensile strength, several reinforcing fillers, such as Indian grass fiber, chitin whisker, and kraft lignin have been studied for an SPI/plasticizer system.[7–9] Lignin macromolecules are inclined to aggregate together and provide supramolecular structures, and can be considered as polydisperse network polymer.[10,11] Alkaline lignin (AL), a by-product from the alkaline pulping process of papermaking, is a high-performance reinforcing filler for synthetic polymer on account of its multifunction, high-impact-strength, thermal resistance, and biodegradable properties.[12–14] However, the reaction activity of AL is relatively low because of the scarcity of active positions within the lignin macromolecular structure. Much of the work related to polymer–lignin products has since focused on increasing the reactivity of the lignin by modifying specific reactive groups, such as carboxyl and hydroxypropyl groups.[15,16] Especially, hydroxyalkylation of lignin has been recognized as a promising technique for overcoming the frequently observed adverse effect of lignin on mechanical properties of solid polymer materials.[17]

Dispersing nanoscale fillers, such as particles and whiskers, in polymer matrix is an effective way to significantly improve the mechanical properties of polymer material, as a result of the strong interfacial interactions and restriction of macromolecular chains.[18–21] Introducing nanoscale lignin microstructures into SPI matrix could be expected as a simple and convenient strategy to reinforce SPI plastics and retain biodegradability. To improve the compatibility, a compatibilizer is usually added to soy protein/polymer systems to increase the interfacial adhesion of the blend.[4,8,22] Glutaraldehyde (GA) is well known for its

Correspondence to: L. Zhang (lnzhang@public.wh.hb.cn).
Contract grant sponsor: National Natural Science Foundation of China; contract grant numbers: 59933070, 20474048.
Contract grant sponsor: Chinese Academy of Sciences.

TABLE I
Components of SPI by TGA, Amino Acid Analysis, and HPLC

Components	Content (%)
Moisture	5.01
Protein	92.32 (drybasis)
Glutamate	18.68
Aspartate	11.38
Leucine	7.39
Arginine	7.05
Lysine	5.77
Isoleucine	5.11
Proline	5.01
Serine	4.73
Phenylalanine	4.50
Valine	4.13
Alanine	4.06
Glycine	3.71
Threonine	3.43
Tyrosine	3.37
Histidine	2.10
Methionine	1.00
Cysteine	0.91

ability to react with protein and lignin.[23–25] This suggests its potential to be a compatibilizer for soy protein/lignin system. In the present work, a series of biodegradable composites were prepared from SPI and hydroxypropyl alkaline lignin (HPL) with GA as compatibilizer. The structure and properties of the SPI/HPL composites were characterized by Fourier transform infrared spectroscopy (FTIR), X-ray diffraction (XRD), differential scanning calorimetry (DSC), dynamic mechanical thermal analysis (DMTA), scanning electron microscopy (SEM), transmission electron microscopy (TEM), and tensile tests. The main purpose of this article is to bring forward a new method to disperse HPL in SPI matrix at a nanoscale and to reinforce soy protein materials.

EXPERIMENTAL

Materials

Commercial SPI was purchased from Dupont-Yunmeng Protein Technology Co. (Yunmeng, People's Republic of China). The weight-average molecular weight (M_w) of SPI was determined, by a multi-angle laser light scattering instrument (Malls, Dawn® DSP, Wyatt Technology Co., Santa Barbara, CA, USA) equipped with a He-Ne laser ($\lambda = 632.8$ nm), to be 2.05×10^5.[26] The moisture content, protein content, and amino acid compositions of SPI were analyzed by thermogravimetric analysis (TGA, TG 209, Netzsch Co., Germany), Kjeletc1030 self analyzer (Switzerland) according to the semimicro Kjeldahl principle, and high performance liquid chromatography (HPLC, Waters), and the results are shown in Table I. Straw AL was supplied by the Key Laboratory of Cellulose Chemistry in Guangzhou Institute of Chemistry, Chinese Academy of Sciences. Propylene oxide, hexane, NaOH, hydrochloric acid, and glycerol were all of analytical grade and were purchased from the Shanghai Chemical Co. (Shanghai, People's Republic of China). Analytical grade GA was a 25% aqueous solution, and was purchased from Shantou Xilong Chemical Plant (Guangdong, People's Republic of China).

Synthesis of HPL

HPL was prepared according to a process developed by Glasser et al.,[27] with modification. AL (20 g) was dissolved in 300 mL of 0.1*M* NaOH aqueous solution, and then the dark-brown AL solution was introduced into a three-necked flask. Propylene oxide (30 g) was added into the AL solution with mechanical stirring for 10 h. The reaction temperature was controlled to be 30 ± 1°C. At the end of the reaction, the viscous reaction mixture was acidified to pH 2 using 1*M* hydrochloric acid, and then was centrifuged at 10,000 rpm for 15 min to obtain the HPL precipitate. The resulting product was washed by hexane three times and vacuum-dried.

Preparation of SPI/HPL composites

SPI (8 g) was dissolved in 200 mL of 0.01*M* NaOH aqueous solution, and then 0, 2, 4, 6, 8, 10, and 12 wt % HPL (the content of HPL in total mass of SPI and HPL) was added, respectively, with mechanical stirring to obtain a homogenous solution. One milliliter of GA (3.3 wt % as the percentage of the GA content in the total mass of SPI, HPL, and GA) was added with continuous mechanical stirring for 0.5 h at a controlled reaction temperature of 60 ± 1°C. In the end, hydrochloric acid was added, adjusting pH to be 3.8. The acidified solution with a precipitate of SPI/HPL composite was centrifuged at 10,000 rpm for 15 min. The resulting composite was washed with diluted hydrochloric acid (pH = 3.8) three times, and then freeze-dried. This series of samples (H-series) were labeled as H-0, H-2, H-4, H-6 H-8, H-10, and H-12 corresponding to 0, 2, 4, 6, 8, 10, and 12 wt % HPL, respectively. By using the aforementioned preparation process, but by fixing the HPL content of 6 wt % and varying the amount of GA added, another series of SPI/HPL composites (G-series) was prepared. The resulting samples were labeled as G-0, G-0.5, G-1, G-2, and G-4 corresponding to 0, 0.5, 1, 2, and 4 mL GA additions (0, 1.7, 3.3, 6.6, and 13.2 wt %), respectively.

Preparation of SPI/HPL plastic sheets

The SPI/HPL composites with a glycerol content of 30 wt % was first mixed in a kitchen beater (HR1704,

Philips, Zhuhai, People's Republic of China) for 15 min, and then mixed with a single-screw extruder (PolyDrive with Rheomex R252, ThermoHaake, Germany, with diameter 19.1 mm and length/diameter of 25:1). The screw rotation speed was 30 rpm, and the temperature profile along the extruder barrel was 80, 100, and 120°C (from feed zone to exit). This process was repeated four times. Subsequently, the resulting mixture was placed in a mold covered with two polished stainless-steel plates, and then compression-molded with a hot press, according to our previous method.[3] The sheets were molded at 140°C under a pressure of 20 MPa for 10 min and then air-cooled to 50°C under constant pressure with a cooling rate of about 3°C min^{-1} before the removal from the mold. All of the samples obtained were conditioned in desiccators, with P_2O_5 as desiccant, for 1 week at room temperature before characterization.

Characterization

FTIR spectra of SPI/HPL composites were recorded on an FTIR spectrometer (1600, Perkin–Elmer Co., MA) in a range of wavenumbers from 400 to 4000 cm^{-1} using KBr pellets. XRD patterns were recorded on the X-ray diffractometer equipped on a D/max-1200 instrument (Rigaku Denki, Japan) with Cu Kα radiation (λ = 0.154 nm). Diffraction data were collected from 2θ = 4°–40° in a fixed time mode with a step interval of 0.10°.

TEM was performed with a Hitachi H-600 electron microscope at 75 kV. Each sample was embedded in an epoxy resin. Ultrathin sections were obtained via sectioning on an LKB-8800 ultratome. SEM was carried out on a Hitachi *S*-570 scanning electron microscope. The sheets in the dry state were frozen in liquid nitrogen, snapped immediately, and then vacuum-dried. The fracture surfaces (the cross sections) of the sheets were sputtered with gold, and then observed and photographed. Optical transmittance (T_r) of the sheets was measured with a UV–vis spectrophotometer (Shimadzu UV-160A, Japan) at a wavelength of 800 nm. The thicknesses of the sheets were ~0.33 mm.

DSC analysis was carried out on a DSC-204 apparatus (NETZSCH Co., Germany) equipped with a liquid-nitrogen cooling system, and was calibrated with an indium standard (T_f = 156.6°C). Each conditioned sample (about 13 mg) was placed in a pressure-tight aluminum capsule, and scanned from −80 to 150°C under nitrogen atmosphere with a heating rate of 20°C min^{-1}. The glass transition temperature (T_g) was taken as the mid-point of the specific heat increment at glass transition. DMTA was performed on a dynamic mechanical thermal analyzer (DMTA-V, Rheometric Scientific Co., Piscataway, NJ, USA) at a frequency of 1 Hz. The specimen was a rectangular strip (30 × 10 × 0.3 mm^3), and the test temperature ranged from −80 to 150°C with a heating rate of 5°C min^{-1}. The α-relaxation temperature (T_α) was determined as the peak value of loss angle tangent (tan δ).

The tensile strength (σ_b), elongation at break (ε_b), and Young's modulus (E) of the sheets were measured on a universal tensile testing machine (CMT6503, Shenzhen SANS Test Machine Co., Shenzhen, People's republic of China) with a tensile rate of 5 mm min^{-1} according to ISO6239–1986 (E). An average value of five replicates of each sample was taken.

RESULTS AND DISCUSSION

FTIR spectra of AL, HPL, SPI, H-0, H-12, and the mixture of SPI and HPL (SPI + HPL) are shown in Figure 1. Comparing HPL with AL, the O—H stretching band of AL at 3404 cm^{-1} distinctly shifts to the one of HPL at 3374 cm^{-1} as a consequence of hydroxypropylation, and is attributed to the increase of hydrogen bonding with the introduction of flexible polypropylene glycol side-chains. The multiplicity, and broadening of the —OCH_3 stretching band at about 2933 cm^{-1} and of the —O— stretching band at about 1120 cm^{-1} for HPL suggest the occurrence of new alkoxy groups and ether linkages after hydroxypropylation. The bands at about 1600, 1500, and 834 cm^{-1} are assigned to aromatic skeletal vibration and the one around 1460 cm^{-1} is assigned to aliphatic C—H bending.[28,29] The FTIR spectrum of HPL is consistent with that reported,[28] confirming the successful synthesis of HPL. In the FTIR spectra of SPI, the broad band at 3292 cm^{-1} is assigned to N—H stretching and three sharp absorption bands at 2960, 2929, and 2875 cm^{-1} are related to the protein antisymmetric and symmetric C—H stretching. The amide I (mainly C═O stretching) is observed as a strong band at 1656 cm^{-1}, with the amide II at 1541 cm^{-1}.[30,31] After being crosslinked by GA, the band of N—H stretching of H-0 is broadened and shifts to 3307 cm^{-1}, attributed to the decrease of —NH_2 as a result of the crosslinking. The possible crosslinkage exists in the intermolecules of SPI/SPI, HPL/HPL, and SPI/HPL for SPI/HPL systems, and crosslinking that has occurred among —NH_2 (arginine, asparagines, and lysine of soy protein) and —OH (tyrosine and serine of SPI and hydroxypropyl groups of HPL) on the basis of the data in Table I. So imine, quaternary ammonium, acetal or/and hemiacetal should exist in the SPI/HPL composites,[32–35] confirmed by the band of —O—C—O— at 1126 cm^{-1} and the band of quaternary ammonium at 1384 cm^{-1} in the spectra of H-0 and H-12, which are absent in the spectra of SPI and HPL. SPI-HPL copolymer could play an important role in the compatibilization of SPI/HPL composites. These results suggest the occurrence of chemical crosslinking network structures in the composites. The restriction of hydrogen bonding in H-0, among amide groups by crosslinking,

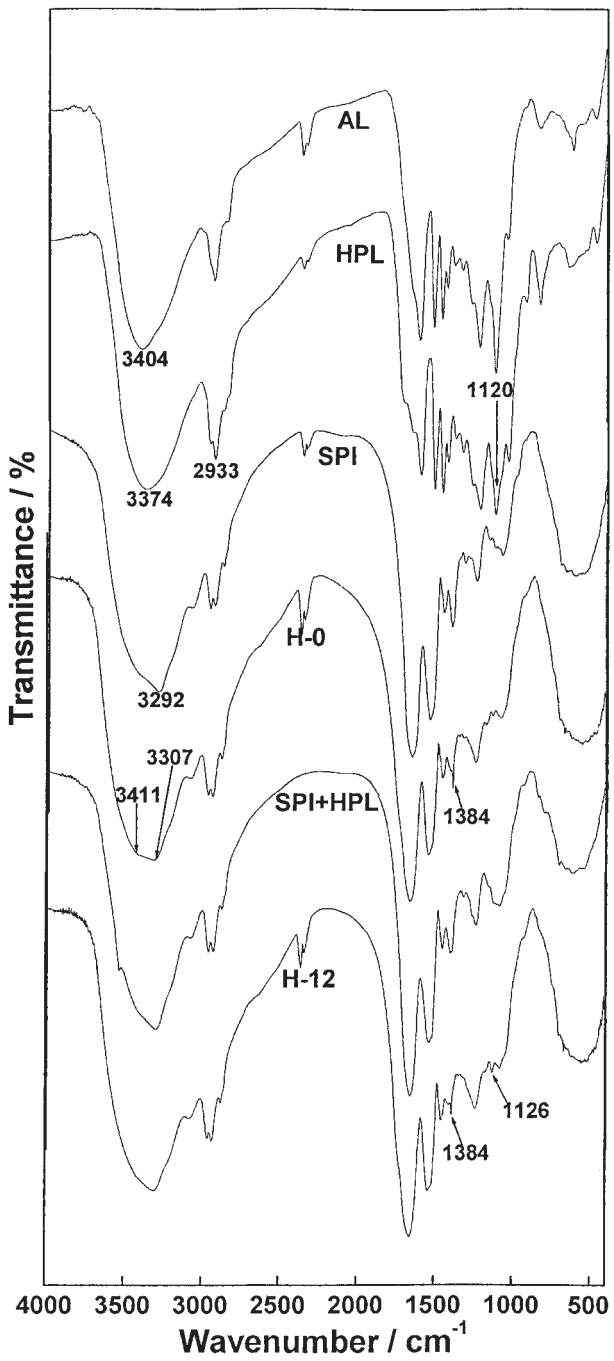

Figure 1 FTIR spectra of AL, HPL, SPI, H-0, H-12, and the mixture of SPI and HPL (SPI + HPL).

leads to the increase of free acylamino groups and the increase of the absorption intensity of free N—H stretching band at 3411 cm^{-1}. After the addition of HPL in H-12, the intensity of this stretching band decreases, indicating that HPL forms strong hydrogen bonding with SPI. Figure 2 exhibits the typical XRD profiles of the SPI/HPL composites. It provides the information that the composites H-0 to 12 with different HPL contents are in the amorphous state.

The TEM images of the H-0, H-2, H-6, and H-12 sheets are shown in Figure 3. The dark spots in the images represent the HPL particles, because of the higher electron density of HPL than SPI, and the area of these dark spots increases with the increase of HPL content. Clearly, HPL disperses in SPI matrices as small particles with a diameter of about 50 nm on the whole, as shown in Figure 3(b)–(d). Interestingly, the number of particles increases, whereas the particles still maintain the diameter of about 50 nm for the H-2 and H-6 sheet, with an increase of HPL content of 2–6 wt % as shown in Figure 3(b) and (c), indicating that HPL nanoparticles homogeneously disperse in the matrix without further aggregation. Lignin tends to form supramolecular structures as a result of the polyfunctionality and strong inter- and intramolecular interactions,[10,36] which suggests that HPL particles are attributed to the supramolecular structures of HPL.[11,37,38] Moreover, the interface of HPL nanoparticles and matrices are indistinct, suggesting a strong interfacial interaction. The small dimension of HPL particles dispersing in SPI matrices proves the effectivity of blending HPL and SPI in the solution state and the compatibilization by GA. When HPL content increases to 12 wt %, some larger particles, with dimensions of more than 100 nm, occur in the H-12 sheet as shown in Figure 3(d), suggesting the further aggregation of HPL. The sharper interface and larger dimension of these particles could imply relatively low interfacial adhesion. Figure 4 shows the SEM images of cross sections of the H-series sheets. The H-0 sheet without HPL exhibits a relatively smooth cross section as shown in Figure 4(a). The cross sections of H-2 and H-6 [shown in Fig. 4(b) and (c)] display homogenous granular structures, suggesting the reinforced interfacial adhesion and certain degree of compatibility, as a result of nanoscale dispersion of HPL. The sparse distribution of grain-like structure, in the cross section shown in Figure 4(d), suggests relatively low interfa-

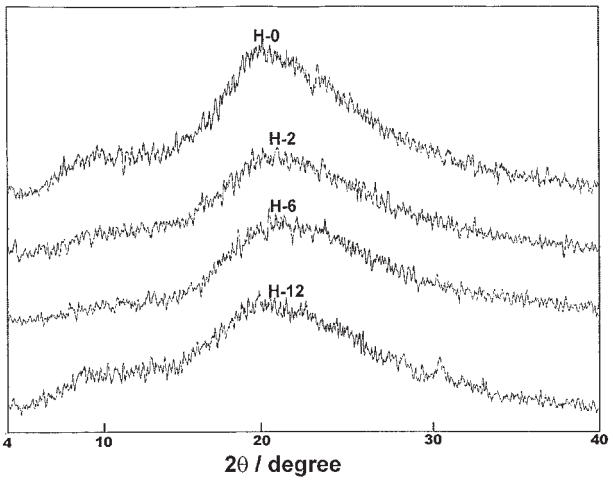

Figure 2 XRD profiles of the H-0, H-2, H-6, and H-12 composites.

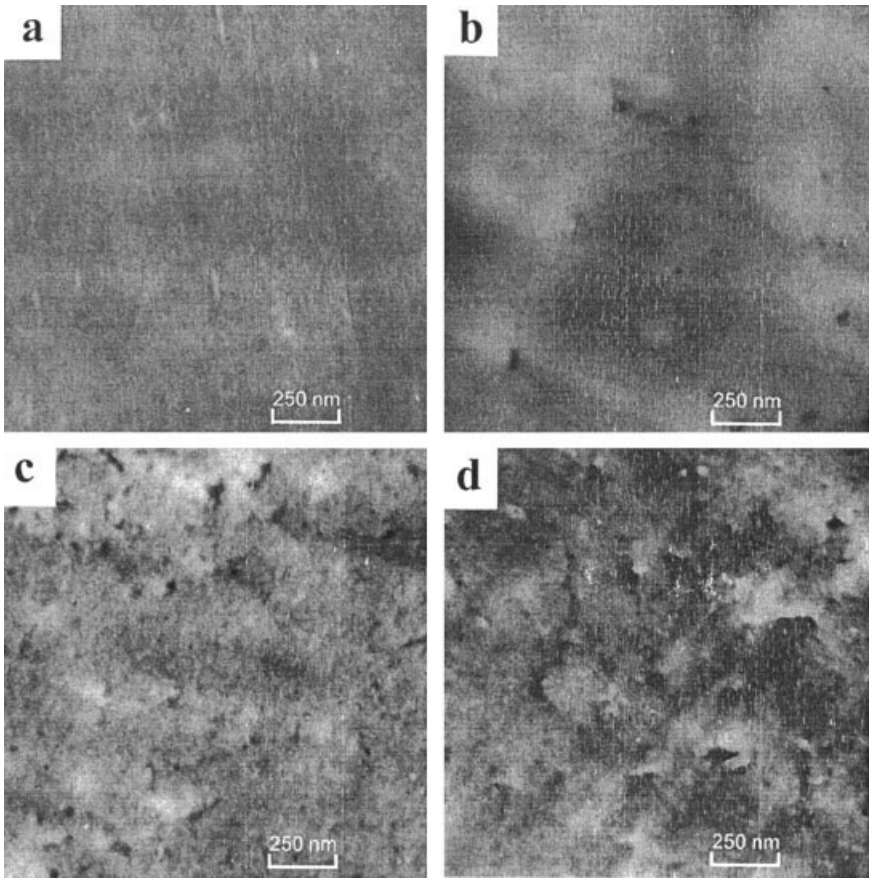

Figure 3 TEM micrographs of the sheets H-0 (a), H-2 (b), H-6 (c), and H-12 (d).

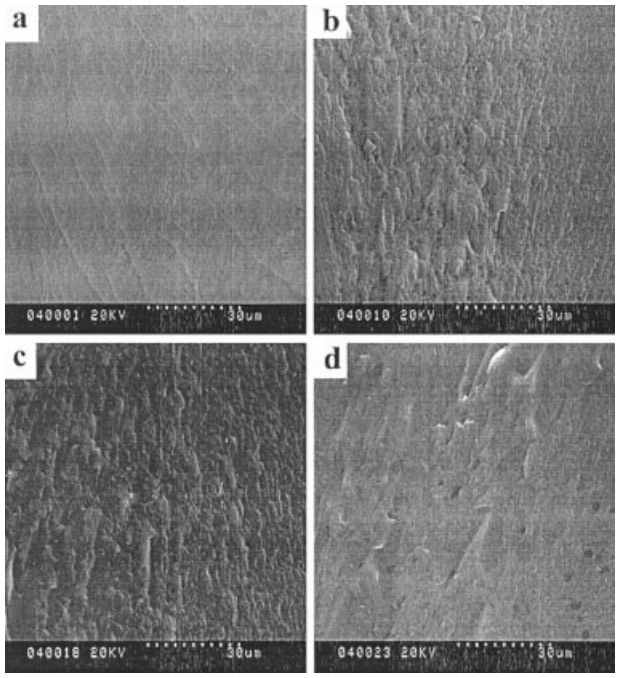

Figure 4 SEM micrographs of the cross sections of the sheets H-0 (a), H-2 (b), H-6 (c), and H-12 (d).

cial adhesion in the H-12 sheets. Usually, the transparency of the sheet is an auxiliary criterion to judge the miscibility of the composite materials.[39] The optical transmittance (T_r) of the dark-brown H-series sheets at the wavelength of 800 nm is shown in Figure 5. With an increase of HPL addition from 0 to 12 wt %, the T_r of H-series sheets at 800 nm slightly decrease from

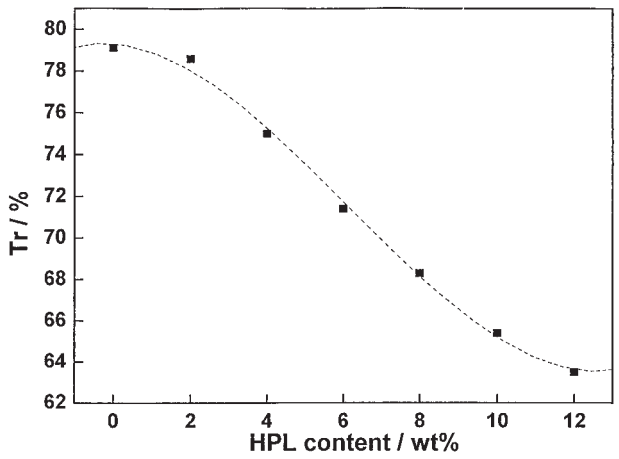

Figure 5 Optical transmittance (T_r) of the H-series sheets at 800 nm.

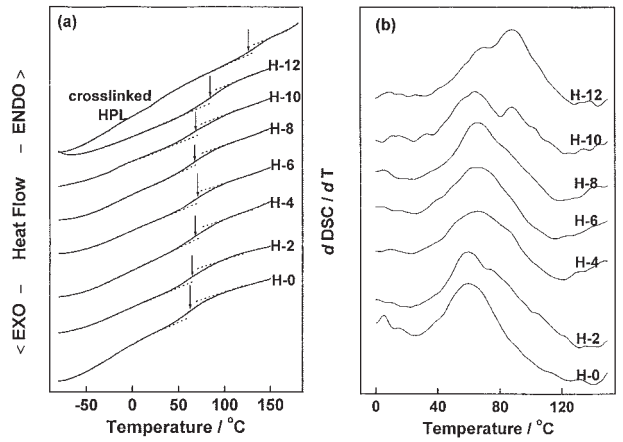

Figure 6 DSC thermograms (a) and dDSC/dT curves (b) of the crosslinked HPL with 30 wt % glycerol as plasticizer and the sheets H-0 to H-12 with various HPL contents. The dash lines and arrows are herein used to point out the glass transition and T_g.

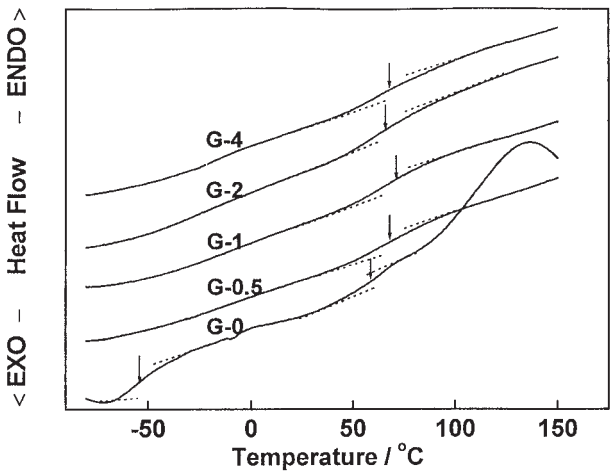

Figure 7 DSC thermograms of the sheets G-0 to G-4 with various GA addition contents. The dash lines and arrows are herein used to point out the glass transition and T_g.

79.1 to 63.5%. The results show that the SPI/HPL sheets are basically transparent, and further confirm that there is no obvious phase separation in the HPL/SPI composite sheets.

The DSC thermograms of the crosslinked HPL and the H-0 to H-12 sheets, with various HPL contents, are shown in Figure 6(a). H-0 without HPL has a glass transition at 62.5°C. With an increase of HPL content, T_g's of H-2 to H-12 increase from 64.2 to 85.1°C. This indicates the introduction of nanoscale HPL into SPI-GA networks can form intermolecular interactions, such as hydrogen bonding, detected by FTIR, leading to the increase of T_g. It is difficult to distinguish the glass transition of HPL domains in the DSC thermograms, but the double peaks around 70 and 90°C in the differential curves of DSC thermograms of H-10 and H-12, shown in Figure 6(b), illustrate the existence of two glass transitions assigned to the protein matrices and HPL domains. These results suggest that the excessive HPL could form larger aggregates when HPL contents increase from 6 to 12 wt %,[40,41] which has been proved by TEM. For all H-series sheets, the glass transition of crosslinked HPL at 126.0°C was absent, indicating that no obvious phase separation occurs in H-series sheets. Figure 7 shows the DSC thermograms of the G-0 to G-4 sheets with various GA additions. There are two glass transitions at −54.0 and 58.7°C for G-0, suggesting that the structure of uncrosslinked SPI/HPL sheets are similar to SPI with 30 wt %.[42,43] With an increase of GA content, T_g's of G-0.5 to G-4 increase and range from 68.2 to 70.4°C, as a result of the network structures caused by crosslinking with GA. In general, the crosslinking effect of GA helps to increase the T_g of the sheets. However, excessive GA could act as a plasticizer, and insufficient addition of GA could cause incomplete crosslinking and the decrease of T_g.[44]

The DMTA spectra of the H-0 to H-12 sheets, plotted in the form of tan δ versus temperature, are presented in Figure 8(a). The relaxation peaks at around 100°C are attributed to the segmental motion of SPI/HPL composites. The α-relaxation temperatures (T_α) of H-0 to H-6 increase from 101.8 to 112.4°C with an increase of HPL content, suggesting HPL nanoparticles restrict the protein network structures. Interestingly, T_α of H-8 drops to 104.6°C, and T_α of H-8 and H-12 increase from 104.6 to 115.0°C. When HPL content increases from 2 to 6 wt %, the number of the particle increases with an invariable dimension of 50 nm, leading to an increase of reinforcing effect and an increase of T_g and T_α. When HPL content is continuously increased from 6 to 12 wt %, on one hand, HPL dispersion appears to form larger domains with a dimension of more than 100 nm: this leads to a de-

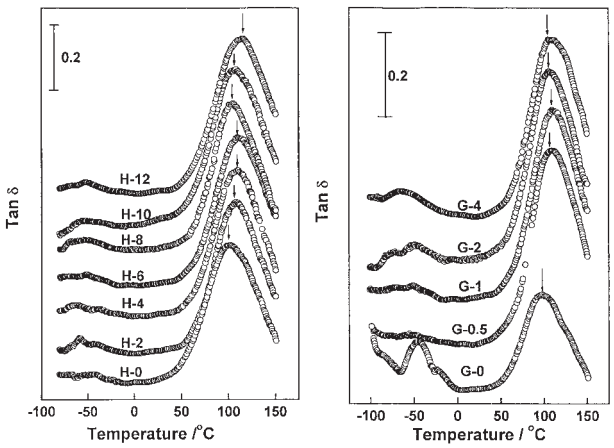

Figure 8 DMTA spectra of the H-series (a) and G-series (b) sheets plotted in the form of tan δ versus temperature. The arrows are herein used to point out T_α.

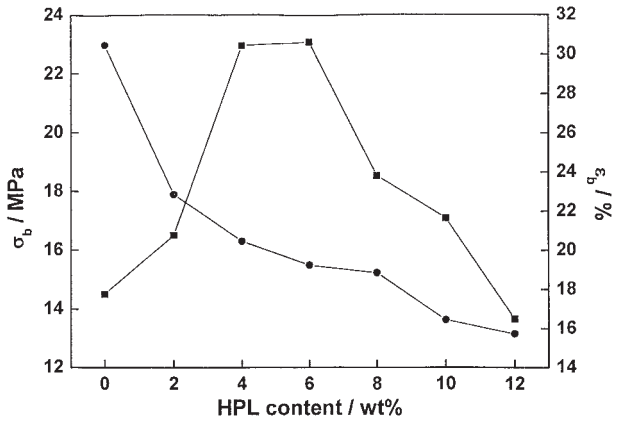

Figure 9 σ_b (■), ε_b (●) of the H-series sheets dependent on the HPL content.

crease of interfacial adhesion and the weakening effect on the restriction of protein segmental mobility. On the other hand, the T_α or T_g of HPL domains occur more and more separately, shown as the double peaks in *d*DSC curves of H-10 and H-12 and broadening of tan δ. These two effects cause the apparent T_g and T_α of H-6 to H-12 first to decrease and then increase with an increase of HPL content. Figure 8(b) shows the DMTA spectra of the G-series sheets. There are two relaxations in the G-0 sheet at −54.0 and 98.7°C. G-1 exhibits the highest value of T_α. It is axiomatic that the α-relaxation reflects the glass transition.[45] However, T_α from DMTA is higher than T_g from DSC, which is assigned to the nature of dynamics in DMTA itself.[46] The results of DMTA further confirm the results from DSC, declaring the most restricted mobility of protein segments in the H-6 sheet and the occurrence of HPL aggregates when HPL content is higher than 6 wt %.

The tensile strength (σ_b) and elongation at break (ε_b) of the H-series sheets are dependent on the HPL content as shown in Figure 9. σ_b and ε_b of the sheet prepared from pure SPI and 30 wt % glycerol as a control are 8.4 MPa and 61.8%, respectively. For H-0 to H-6, σ_b significantly increases from 14.5 to 23.1 MPa, in which H-6 possesses σ_b as much as 2.8-fold over that of the control and 1.5-fold over H-0 without HPL addition. HPL particles at the nanoscale, as well as the network structures of SPI/HPL composites play an important role in the improvement of σ_b. The decrease of σ_b and E of H-8 to H-12 indicates the presence of structural defects caused by HPL particles with a diameter of more than 100 nm. ε_b of the sheets H-0 to H-12 slightly decrease from 33.4 to 19.2%, and is ascribed to the restriction on SPI molecular segments by HPL. The relationships of mechanical properties and GA addition are shown in Figure 10. The G-0 sheets, without the addition of GA, exhibit relatively low σ_b and ε_b compared with G-0.5 to G-4. When the GA added is 0.5 mL, namely 1.7 wt %, the compatibilization of GA leads to a significant increase of σ_b and ε_b. From the results of the H- and G-series, σ_b of H-1 to H-12 and G-0.5 to G-4 composite sheets are higher than those of the pure SPI sheet without HPL and GA (the control), GA crosslinked SPI without HPL (H-0), and SPI/HPL composite sheet without GA (G-0). It is believable that the increase of σ_b for H-series sheets is attributed to physical crosslinking between nanoscale dispersed HPL and the SPI matrix. In the same way, the enhancement of the mechanical properties of the G-series sheets is related to the occurrence of complex networks crosslinked by GA. The G-1 (or H-6) sheet prepared with the addition of 3.3 wt % GA and 6 wt % HPL possesses the best mechanical properties in this case. This work provides a novel way to use nanoscale lignin particles to reinforce the soy protein plastics.

CONCLUSIONS

HPL has been homogeneously dispersed in SPI as nanoparticle with GA as compatibilizer to improve the mechanical properties. The compression-molded plastic sheets from SPI, 6 wt % HPL and 3.3 wt % GA exhibited better mechanical properties than those without HPL addition. The results of FTIR and XRD indicated that SPI/HPL composites are of amorphous network structure and resulted from the physical crosslinking between HPL and SPI as well as the chemical crosslinking with GA between SPI/SPI, HPL/HPL, and SPI/HPL. TEM micrographs demonstrate that the compatibilization of GA leads to small dimension of the dispersed HPL particles being about 50 nm in diameter. The cross section of the H-series sheets with dense grain-like structures confirms good interfacial adhesion of the SPI/HPL composites. The restricting effects of nanoscale HPL particles on the network structures in the SPI/HPL sheets are responsible for the increase of T_g from 62.5 to 70.4°C of the SPI/HPL sheets when HPL content increases from 0 to

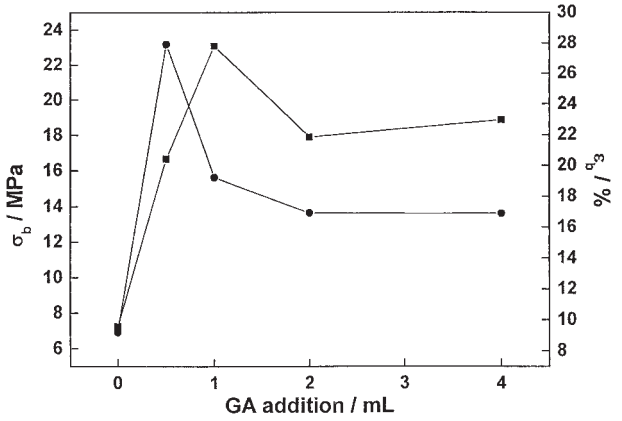

Figure 10 σ_b (■) and ε_b (●) of the G-series sheets dependent on the GA addition.

6 wt % and a similar changing tendency of T_α is observed. Furthermore, this microstructure results in an obvious improvement of mechanical and thermal properties.

References

1. Chiellini, E.; Cinelli, P.; Chiellini, F.; Imam, S. H. Macromol Biosci 2004, 4, 218.
2. Mo, X.; Sun, X. S.; Wang, Y. J Appl Polym Sci 2001, 73, 2595.
3. Wu, Q.; Zhang, L. Ind Eng Chem Res 2001, 40, 1879.
4. Zhong, Z.; Sun, X. S. Polymer 2001, 42, 6961.
5. Zhang, J.; Mungara, P.; Jane, J. Polymer 2001, 42, 2569.
6. Wang, S.; Sue, H. J.; Jane, J. Pure Appl Chem 1996, 33, 557.
7. Lu, Y.; Weng, L.; Zhang, L. Biomacromolecules 2004, 5, 1046.
8. Huang, J.; Zhang, L.; Wei, H.; Cao, X. J Appl Polym Sci 2004, 93, 624.
9. Liu, W.; Mohanty, A. K.; Askeland, P.; Drzal, L. T.; Misra, M. Polymer 2004, 45, 7589.
10. Karmanov, A. P.; Monakov, Y. B. Russ Chem Rev 2003, 72, 715.
11. Li, Y.; Sarkanen, S. Macromolecules 2002, 35, 9707.
12. Wang, J.; Manley, R. J.; Feldman, D. Prog Polym Sci 1992, 17, 611.
13. Meister, J. J.; Patil, D. R. Macromolecules 1985, 18, 1559.
14. Chen, M. J.; Gunnells, D. W.; Gardner, D. J.; Milstein, O.; Gersonde, R.; Feine, H. J.; Hüttermann, A.; Frund, R.; Lüdemann, H. D.; Meister, J. J. Macromolecules 1996, 29, 1389.
15. Feldman, D.; Lacasse, M.; Beznaczuk, L. M. Prog Polym Sci 1986, 12, 271.
16. Oliveira, W. D.; Glasser, W. G. Macromolecules 1994, 27, 5.
17. Wu, L. C.; Glasser, W. G. J Appl Polym Sci 1984, 29, 1111.
18. Park, H. M.; Misra, M.; Drzal, L. T.; Mohanty, A. K. Biomacromolecules 2004, 5, 2281.
19. Rong, M. Z.; Zhang, M. Q.; Zheng, Y. X.; Zeng, H. M.; Walter, R.; Friedrich, K. Polymer 2001, 42, 167.
20. Incarnato, L.; Scarfato, P.; Russo, G. M.; Di Maio, L.; Iannelli, P.; Acierno, D. Polymer 2003, 44, 4625.
21. Mathew, A. P.; Dufresne, A. Biomacromolecules 2002, 3, 609.
22. Koning, C.; Duin, M. V.; Pagnoulle, C.; Jerome, R. Prog Polym Sci 1998, 23, 707.
23. Marquié, C. J Agric Food Chem 2001, 49, 4676.
24. Park, S. K.; Bae, D. H.; Rhee, K. C. J Am Oil Chem Soc 2000, 77, 879.
25. Yamamoto, H.; Amaike, M.; Saitoh, H.; Sano, Y. Mater Sci Eng C 2000, 7, 143.
26. Wu, Q.; Zhang, L. J Appl Polym Sci 2001, 82, 3373.
27. Glasser, W. G.; Wu, L. C.; Selin, J. F. Wood and Agricultural Residues—Research on Use for Feed, Fuels and Chemicals; Soltes, E. J., Ed.; Academic: New York, 1983, p 149.
28. Glasser, W. G.; Barnett, C. A.; Rials, T. G.; Saraf, V. P. J Appl Polym Sci 1984, 29, 1831.
29. Nada, A. M. A.; Yousef, M. A.; Shaffei, K. A.; Salah, A. M. Polym Degrad Stab 1998, 62, 157.
30. Nahar, S.; Tajmir-Riahi, H. A. J Colloid Interface Sci 1996, 178, 648.
31. MacDonald, G. M.; Barry, B. A. Biochemistry 1992, 31, 9848.
32. Whipple, E. B.; Ruta, M. J Org Chem 1974, 39, 1666.
33. Tashima, T.; Imai, M.; Kuroda, Y.; Yagi, A.; Nakagawa, T. J Org Chem 1991, 56, 694.
34. Margel, S.; Rembaum, A. Macromolecules 1980, 13, 19.
35. Rogers, J. D. Environ Sci Technol 1989, 23, 177.
36. Micic, M.; Benitez, I.; Ruano, M.; Mavers, M.; Jeremic, M.; Radotic, K.; Moy, V.; Leblanc, R. M. Chem Phys Lett 2001, 347, 41.
37. Micic, M.; Radotic, K.; Jeremic, M.; Leblanc, R. M. Macromol Biosci 2003, 3, 100.
38. Micic, M.; Radotic, K.; Benitez, I.; Ruano, M.; Jeremic, M.; Moy, V.; Mabrouki, R. M.; Leblanc, M. Biophys Chem 2001, 94, 257.
39. Krause, S. J Macromol Sci Rev Macromol Chem 1972, 2, 251.
40. Siochi, E. J.; Ward, T. C.; Haney, M. A.; Mahn, B. Macromolecules 1990, 23, 1420.
41. Norgren, M.; Edlund, H.; Wågberg, L. Langmuir 2002, 18, 2859.
42. Chen, P.; Zhang, L. Macromol Biosci 2005, 5, 237.
43. Chen, P.; Zhang, L.; Cao, F. Macromol Biosci 2005, 5, 872.
44. Zhang, L.; Chen, P.; Huang, J.; Yang, G.; Zheng, L. J Appl Polym Sci 2003, 88, 422.
45. Zeng, M.; Zhang, L.; Zhou, Y. Polymer 2004, 45, 3535.
46. Rieger, J. Polym Test 2001, 20, 199.